PCCP

Accepted Manuscript

ROYAL SOCIETY OF CHEMISTRY

www.rsc.org/pccp

Journal Name

RSCPublishing

ARTICLE

Enhanced dye-sensitized solar cell photocurrent and efficiency using a Y-shaped, pyrazine-containing heteroaromatic sensitizer linkage

Cite this: DOI: 10.1039/x0xx00000x

Received 00th January 2012,
Accepted 00th January 2012

DOI: 10.1039/x0xx00000x

www.rsc.org/

Brian L. Watson,[a] Benjamin D. Sherman,[a] Ana L. Moore,[a]* Thomas A. Moore,[a]* Devens Gust[a,]*

A new sensitizer motif for dye sensitized solar cells (DSSC) has been developed. A heteroaromatic moiety containing a pyrazine ring links two porphyrin chromophores to the metal oxide surface via two carboxylic acid attachment groups. A test DSSC sensitized with the new molecule was 3.5 times more efficient than a similar cell sensitized by a single porphyrin model compound. The open circuit photovoltage was increased by a modest factor of 1.3, but the photocurrent increased by a factor of 2.7. Most of the increase is attributed to a reduced rate of charge recombination of the charge separated state formed by photoinduced electron transfer from the excited sensitizer to the TiO2, although some of the difference is due to increased light absorption resulting from more dye on the photoanode. Increased light absorption due to the pyrazine group may also play a role. The design illustrated here could also be used to link complementary sensitizers or antenna moieties in order to increase spectral coverage.

Introduction

The first report of the dye sensitized solar cell (DSSC) by O'Regan and Grätzel in 1991[1] has spawned a huge number of studies[2-5] investigating the various cell components, with a view toward improving efficiency. Numerous sensitizer dyes have been investigated, and only a few such studies are cited here.[6-20] One vital component is the linkage joining the sensitizing chromophore to the nanoparticulate wide band gap semiconductor electrode. The nature of this linkage can affect essentially all aspects of the interaction of the dye with the semiconductor and with the redox couple in solution. Although there have been a variety of studies that examine the use of multiple linkers to attach a single chromophore to the oxide surface, there are very few investigations of the use of a single linkage moiety to bind several chromophores to the semiconductor. Here, we report the investigation of a pyrazine-containing heteroaromatic scaffold (PZ) to bind two porphyrin dyes (P) to TiO_2. The porphyrins bear dodecyloxy groups to increase solubility, hinder aggregation of the sensitizers on the metal oxide surface and screen the TiO_2 surface from the electrolyte. The properties of this molecule (**P_2-PZ**, Fig. 1) for sensitization of a DSSC are contrasted with those of a single-porphyrin model sensitizer **P**. Among other things, the substituted pyrazine linkage could affect the binding of the sensitizer to the TiO_2 (because of the presence of two carboxylic acid attachment groups), the rate constants for photoinduced charge injection and charge recombination (because of the aromatic nature of the linkage and its rigid structure), and the surface packing of the sensitizers. In addition, such a sensitizer could be designed to bear either two sensitizer dyes harvesting different spectral regions, or a sensitizer dye and an antenna chromophore that could transfer excitation energy to the sensitizer. The results presented below give the synthesis and the spectroscopic and electrochemical properties of **P_2-PZ** and **P**, and show that in DSSC cells, **P_2-PZ** gives higher photovoltages and strikingly higher short circuit currents and efficiencies than does **P**.

Results and Discussion

Synthesis of sensitizers

Fig. 2 shows the synthetic route to **P_2-PZ**. Condensation of the dipyrromethanes and aldehyde shown in the Figure gave the corresponding porphyrin with a hydrogen atom at a *meso*-position. Zinc was inserted, and treatment of the metalated porphyrin with *N*-bromosuccinimide gave the *meso*-brominated porphyrin. The functionalization of the metalloporphyrin core of **1** was achieved via a palladium-mediated coupling of 4,4,5,5-tetramethyl-1,3,2-dioxaborolane with the brominated porphyrin. The 3,6-porphyrin-functionalized phenanthrene-9,10-dione building block **2** was produced by Suzuki coupling of 3,6-dibromo-9,10-phenanthrenedione with the boronic ester-functionalized porphyrin **1** (step *f*). Next, 4,5-diaminophthalonitrile was condensed with **2** in an acetic acid catalyzed reaction to produce the dinitrile **3** (step *g*). The carboxylic acid functionalities were obtained through acid hydrolysis of the dinitriles (step *h*). The harsh acidic conditions

employed in the hydrolysis resulted in cleavage of some of the dodecyloxy groups. A Williamson ether synthesis was employed to regenerate damaged dye molecules and subsequent base hydrolysis ensured the conversion of any anhydride dehydration product to the free dicarboxylic acid. Synthesis of the control dye **P** was achieved in three steps using standard procedures. Details for all syntheses are reported in the Experimental section.

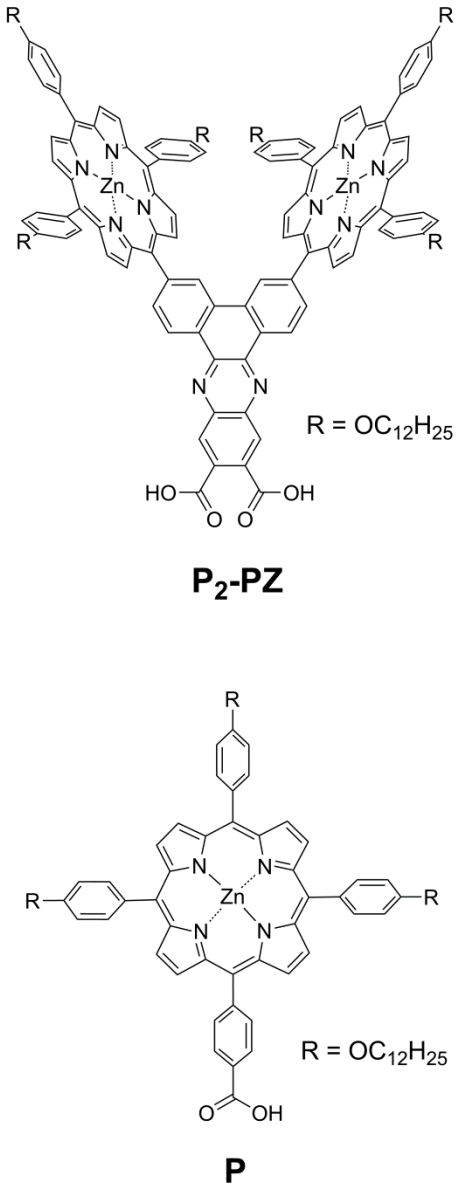

Fig. 1. Structures of the pyrazine-containing heteroaromatic moiety bearing two porphyrin dyes (**P_2-PZ**) and the model porphyrin sensitizer **P**. The dodecyloxy chains confer solubility in organic solvents to the molecules.

Absorption and emission spectra

The absorption and emission spectra of the two dyes are shown in Fig. 3. The spectrum of **P** is typical for a zinc tetraarylporphyrin, with a sharp Soret band at 424 nm and Q-band maxima at 518 (sh), 551 and 591 nm. The spectrum of **P_2-PZ** is dominated by features attributed to the porphyrins, with a Soret band at 421 nm and Q-bands at 552 and 594 nm. The Soret band is significantly broadened relative to that of **P**, and a shoulder has appeared. There is also a ca. 3 nm bathochromic shift of the last Q-band absorption. The shoulder on the Soret absorption at 432 nm is ascribed in part to absorption by the spacer PZ. The broadening of the Soret is attributed to excitonic interaction between the porphyrins, which approach one another relatively closely. The absorption spectrum of **P_2-PZ** contains a small, broad band around 700 nm which is of variable intensity from sample to sample, and might be due to a small amount of the acid anhydride. This component could be removed by refluxing the sample with aqueous potassium hydroxide in tetrahydrofuran, and forms again if the pure material is allowed to stand in solvent at ambient temperatures.

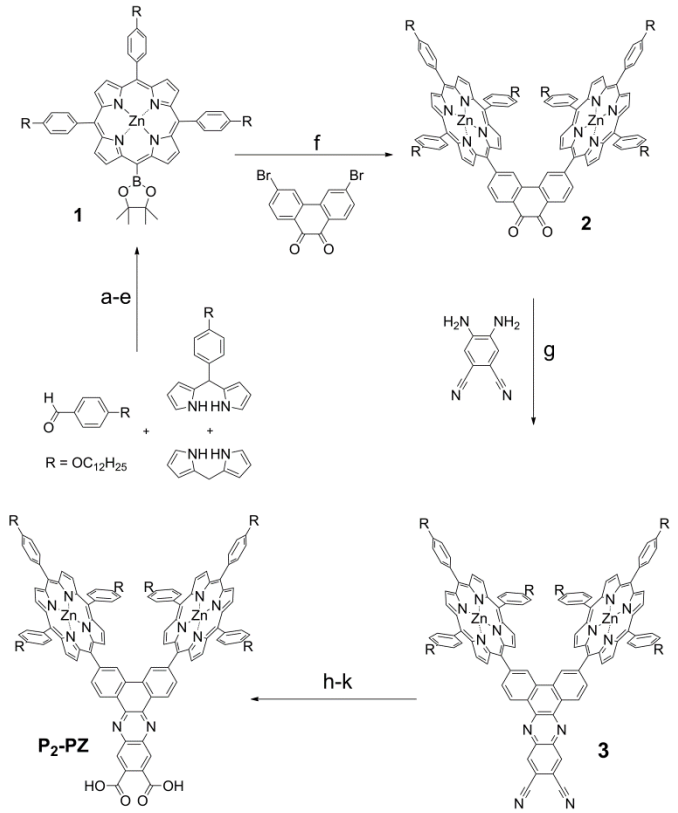

Fig. 2. Synthetic scheme for synthesis of **P_2-PZ**. (a) BF_3•OEt_2, $CHCl_3$, room temperature, 3 h; (b) 2,3-dichloro-5,6-dicyanoquinone, room temperature, 1 h; (c) $Zn(OAc)_2$•$2H_2O$, dichloromethane:MeOH (2:5), reflux overnight; (d) *N*-bromosuccinimide, $CHCl_3$, room temperature, 2 h; (e) 4,4,5,5-tetramethyl-1,3,2-dioxaborolane, $Pd(PPh_3)_2Cl_2$, Et_3N, 1,2-dichloroethane, Ar, reflux overnight; (f) $Pd(PPh_3)_4$, Cs_2CO_3, THF, 90 °C, overnight; (g) AcOH:EtOH:toluene (1:1:2), 100 °C, 20 h; (h) TFA:12 N HCl (1:1), pressure tube, reflux, 6 days. (i) 1-bromododecane, dimethylformamide, K_2CO_3, 70 °C, overnight; (j) $Zn(OAc)_2$, MeOH, dichloromethane, reflux overnight; (k) THF, KOH, H_2O, reflux overnight.

Fig. 3 also shows the fluorescence emission spectra of the two molecules with excitation at 395 nm. Maxima for P are found at 604 and 650 nm, and are characteristic of emission from zinc tetra-arylporphyrins. Dyad **P_2-PZ** shows maxima at 610 and 654 nm. The singlet excited state energies of the two dyes were estimated from the wavenumber average of the

longest-wavelength absorption band and shortest-wavelength emission band in dichloromethane, and are very similar: 2.08 eV for **P** and 2.06 eV for **P_2-PZ**.

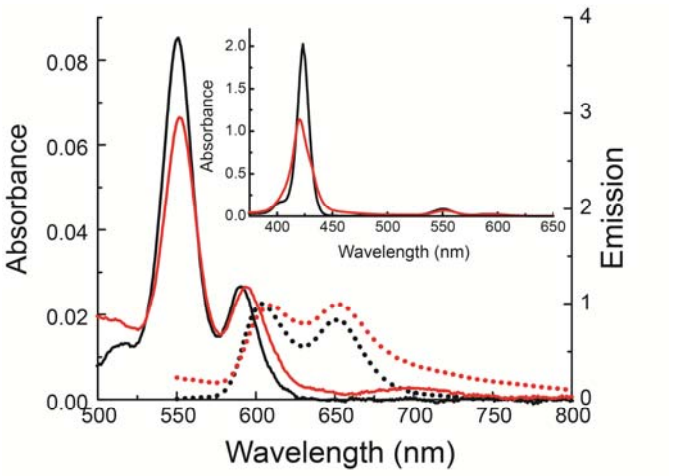

Fig. 3. Absorption (solid) and fluorescence emission with excitation at 395 nm (dotted) spectra of **P** (black) and **P_2-PZ** (red) in dichloromethane solution. The absorption spectra are normalized at the longest-wavelength Q-band, and the emission spectra are normalized at the shortest-wavelength maxima.

Fig. 3 shows that incorporation of the porphyrins into the **P_2-PZ** dyad leads to some small spectral changes due to the close approach of the porphyrin moieties and possibly some weak interaction with the PZ linkage, but does not significantly perturb the porphyrin chromophore.

Dye-sensitized solar cell performance

The DSSCs were constructed with **P** and **P_2-PZ** as sensitizers. The photoanode material was nanoparticulate TiO_2 deposited on fluorinated tin oxide conducting glass. The electrolyte consisted of 1:1 acetonitrile:valeronitrile containing 0.2 M lithium iodide, 0.05 M iodine, 0.2 M tetra-*n*-butylammonium iodide, and 0.5 M 4-*t*-butylpyridine. Excitation was by a xenon arc lamp equipped with AM 1.5 filters, with the cells positioned to receive a light intensity of 100 mW cm^{-2}. Details are given in the Experimental section. These cells were not optimized, and were made thin enough so that the absorbance could be accurately determined. The intent was to compare the performance of the new sensitizer with that of a standard porphyrin sensitizer, rather than to produce high photocurrents.

The absorption spectra of the photoanodes of the respective cells, together with the photocurrent traces, photocurrent vs. applied potential (*J-V)* curves and incident photon to current efficiency (IPCE) spectra are shown in Fig. 4. In the absorption spectra, only the Q-band absorption is shown, as both samples absorb essentially all of the light in the Soret region around 400 nm. The absorption spectra have been corrected for light scatter from the particles of TiO_2 by polynomial modeling of the scatter in a long-wavelength region where the sensitizers do not absorb.[21] Relevant data are summarized in Table 1, where J_{SC} is the short circuit current, V_{OC} is the open circuit voltage, *FF* is the fill factor, and η is the overall solar conversion efficiency. The fill factor is calculated using eq. 1, where V_{MP} is the voltage at the maximum power point and J_{MP} is the photocurrent at this point.

$$FF = \frac{V_{MP}J_{MP}}{V_{OC}J_{SC}} \quad (1)$$

The efficiency η is calculated from eq. 2, where P_{in} is the input power of 100 mW/cm^2.

$$\eta = \frac{V_{OC}J_{SC}FF}{P_{in}} \quad (2)$$

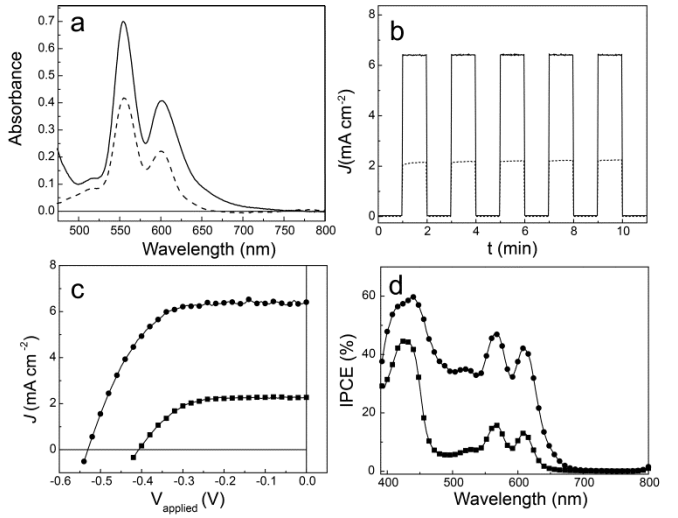

Fig. 4. Performance of DSSC sensitized by model porphyrin **P** and sensitizer **P_2-PZ**. (a) Absorption spectra of photoanodes sensitized by **P_2-PZ** (solid) and **P** (dashed). The spectra have been corrected for light scatter from the nanoparticulate TiO_2. (b) Current produced by DSSC using the photoanodes in (a) for **P_2-PZ** (solid) and **P** (dashed). A xenon arc lamp equipped with an AM 1.5 filter provided illumination at an intensity of 100 mW cm^{-2}, and the DSSC were exposed to alternating 1 min dark and light cycles during the 11 min current trace shown. (c) Current vs. applied voltage plots for the same DSSC sensitized by **P_2-PZ** (circles) and **P** (squares). (d) Incident photon to current efficiencies (IPCE) for the same DSSC sensitized by **P_2-PZ** (circles) and **P** (squares).

It is evident from Fig. 4 and Table 1 that although the two DSSC had comparable fill factors, the cell sensitized by **P_2-PZ** gave somewhat higher V_{OC}, substantially more J_{SC}, and much higher efficiency than that using **P**. The major contributing factor to the increased efficiency was the higher J_{SC} for the **P_2-PZ** cell. We will now consider some of the possible reasons for this difference in behavior.

Table 1. Solar cell performance for **P** and **P_2-PZ**

Property	P	P_2-PZ	P_2-PZ/P
Fraction of light absorbed @ 600 nm	0.40	0.64	1.6
J_{SC} (mA/cm^2)	2.28	6.24	2.7
V_{OC} (V)	0.41	0.53	1.3
FF	0.62	0.60	1.0
η (%)	0.58	2.00	3.5

Light absorption

Fig. 4 shows that in this particular pair of cells, the **P_2-PZ** - sensitized cell had a higher absorbance than the **P** - sensitized cell. At the red-most Q-band, for example, the **P_2-PZ** photoanode absorbed ca. 1.6 times the amount of light absorbed by the **P** electrode. This Q-band maximum, at about 600 nm, was chosen for comparison because any errors due to the scatter correction will be minimized at this longer wavelength, where scatter is decreased. In order to determine whether this difference in the fraction of light absorbed is an inherent property of the adsorbed sensitizers or simply the result of different concentrations of sensitizer in the solutions used to prepare the two slides, a study of sensitizer loading was performed. Solutions of **P_2-PZ** and **P** with equal absorbance at the longest-wavelength Q-band were prepared in dichloromethane. Thus, the **P_2-PZ** solution was ca. half the concentration of the **P** solution, and the concentration of carboxylate binding groups was identical for the two solutions. Identical unsensitized photoanodes were prepared with thin coatings of nanoparticulate TiO_2 in order to facilitate spectroscopic measurements, and their UV-visible spectra (scatter curves) were determined (Fig. 5). Each photoanode was soaked in one of the sensitizer solutions for 18 h, removed from the dye solution and rinsed with the dye solvent, and the absorption spectrum was taken. The results appear in Fig. 5. In the 600 nm region, the absorbance of the electrode bearing **P** is 1.6 times that of the **P_2-PZ** electrode. Carboxyl groups have been found to bind strongly to TiO_2 under the conditions employed,[10,22-26] and we might expect even stronger binding by the dicarboxyl groups of **P_2-PZ**. If we assume that all available carboxylate binding sites on the TiO_2 surface were saturated with sensitizer in both these experiments, then it appears that the larger **P_2-PZ** molecule occupies considerably more space on the metal oxide surface than does **P**, and blocks some potential binding sites, leading to absorption of less than half as many molecules on the surface.

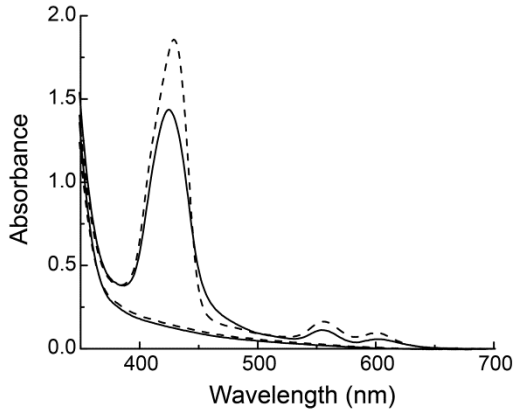

Fig. 5. Absorption spectra of nanoparticulate TiO_2 photoanodes after soaking for 18 h in dichloromethane solutions of equal sensitizer absorbance at 600 nm: dyad **P_2-PZ** and the corresponding scatter curve from the unsoaked electrode (solid) and **P** and the corresponding scatter curve (dashed).

Although formation of non-covalent aggregates of porphyrins in **P**, but not in **P_2-PZ**, could in principle explain these results, this is unlikely because *meso*-tetraarylporphyrins show little tendency to aggregate, and the slides were well rinsed with solvent prior to use.

These experiments show that the absorption difference at 600 nm between the **P** and **P_2-PZ** electrodes used in the cells whose performance is shown in Fig. 4 is not an inherent property of the chromophores, but rather an artifact of the way these cells were prepared. It is evident from the last column in Table 1 that the absorption difference between the electrodes that produced the data in Fig. 4 (the **P_2-PZ** electrode absorbed 1.6 times as much light as the **P** electrode at 600 nm) is not sufficient to account for the large increase in short circuit current of the **P_2-PZ** sensitized cell compared to that sensitized with **P** (a factor of 2.7) or the increase in efficiency (a factor of 3.5).

Redox potentials

Another difference between the two sensitizers that could affect performance is the oxidation potential. The rates of some of the electron transfer reactions that contribute to cell performance – photoinduced charge injection from the dye into TiO_2, charge recombination of the resulting charge-separated state, and electron donation from the reduced solution mediator to the oxidized dye – are functions of this potential. We therefore investigated the redox chemistry of the sensitizers by cyclic voltammetry in dichloromethane containing 0.1 M tetra-*n*-butylammonium hexafluorophosphate as the supporting electrolyte. The working electrode was glassy carbon, the counter electrode was a platinum mesh, and the quasi-reference electrode was Ag^+/Ag. Ferrocene was used as an internal reference, and the measured potentials converted to SCE using a value of 0.45 V for the Fc^+/Fc couple. Details are given in the Experimental section. The cyclic voltammograms are shown in Fig. 6, and relevant potentials are given in Table 2, along with spectroscopic data. The first oxidation potential of **P** is very similar to that of zinc *meso*-tetraphenylporphyrin, and the first oxidation potential of **P_2-PZ** is essentially identical. The energies of the first excited singlet states of the two substances are also essentially identical, and both have ample excited state potential to inject electrons into nanoparticulate TiO_2.[27-29] Thus, the **PZ** linking moiety of **P_2-PZ** does not affect the redox properties of the porphyrins appreciably, and differences in redox behavior cannot be responsible for the difference in performance of the two materials as sensitizers. In addition, the cyclic voltammogram of **P_2-PZ** showed no evidence for oxidation or reduction of the pyrazine-containing linker within the range of potentials exhibited by the porphyrin moieties.

Table 2. Redox (V vs. SCE) and excited state properties of **P_2-PZ** and **P**

Sensitizer	Ox_1	Red_1	Abs_{max} (nm)	Em_{max} (nm)	$E_{(0-0)}$ (eV)
P_2-PZ	0.74	-1.40	594	610	2.06
P	0.76	-1.41	591	604	2.08

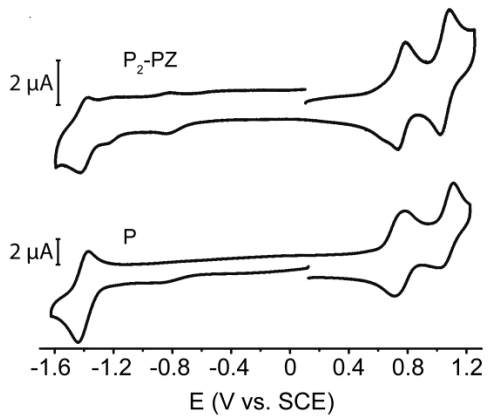

Fig. 6. Cyclic voltammograms for **P_2-PZ** (upper trace) and **P** (lower trace) in dichloromethane. The conditions for obtaining the voltammograms are delineated in the Experimental section.

THE ROLE OF THE PYRAZINE-CONTAINING SPACER

It is clear from the above results that incorporation of the porphyrins into **P_2-PZ** does not materially affect their excited state or redox properties, and that the performance differences noted in Table 1 cannot be explained by any such changes, or simply by differences in surface coverage. The effect of surface coverage differences must be significantly less than might be suggested from the spectra in Fig. 4 and the data in Table 1 because the two electrodes in question had absorbance >1 at all wavelengths less than 450 nm, and thus absorbed essentially all of the light in that region. Thus, the **PZ** linker moiety must affect performance in other ways.

The cyclic voltammetric and spectroscopic results show that the **PZ** linkage is not thermodynamically competent to either accept an electron from the zinc porphyrin excited state or donate an electron to that moiety. Thus, it cannot serve as a discrete intermediate in the process of electron transfer from the excited porphyrin to the TiO_2.

The absorption spectrum of **P_2-PZ** shows that the energy of the first excited singlet state of the **PZ** linkage is above that of the zinc porphyrins, and therefore the zinc porphyrins cannot transfer singlet excitation energy to the linkage. The linkage does absorb some light in regions that could contribute to photocurrent, and may donate this excitation energy to the porphyrin, thus increasing the overall cell efficiency to a relatively small degree via an antenna effect. However, the absorption differences (Fig. 3) are not large enough to account for the dramatically enhanced performance of **P_2-PZ** as compared to **P**. The greatest absorption differences occur in the Soret region around 420 nm, and both photoanodes absorb all of the light in this spectral region.

Thus, the main effect of the pyrazine-containing linker group on cell performance must be due to changes in the rates of the electron transfer processes occurring at the sensitizer-electrode interface. The rate of photoinduced electron transfer from the excited sensitizer to the TiO_2 nanoparticle can limit the yield of photocurrent if that rate is comparable to the rates of other processes that depopulate the excited state. A number of studies indicate that for sensitizers such as **P**, the charge injection rate is on the ps time scale or faster, whereas the excited state lifetimes of related zinc porphyrins are in the range of a few ns.[14,27,30,31] Thus, the quantum efficiency of electron injection in **P** is expected to be near unity (barring aggregation on the surface). Clearly, although the pyrazine linkage in **P_2-PZ** is conjugated and thus could facilitate electron transfer from the porphyrins to the metal oxide relative to a saturated linker of the same length, the transfer rate would still be expected to be slower than that for **P**. The linker could only reduce the IPCE relative to **P**.

Another important electron transfer process is electron donation from the reduced redox couple in solution (I^-) to the oxidized sensitizer. Increasing the rate of this process could lead to an increase in cell efficiency. It is possible that this rate could be faster with **P_2-PZ** than with **P**, but a reason for this is not obvious. For example, **P_2-PZ** might form a ground-state complex of some sort with I^- so that the reaction in question is not limited by diffusion.

It is more likely that the major difference between the performance of **P_2-PZ** and **P** is related to changes in the rate of charge recombination between electrons in the TiO_2 nanoparticle and the oxidized sensitizer. This reaction competes with oxidation of the I^- relay, and slowing it can therefore increase photocurrents. In both $\mathbf{P}^{\bullet+}$ and $[\mathbf{P_2\text{-}PZ}]^{\bullet+}$, the radical cation is centered on a porphyrin moiety. In the case of **P**, the porphyrin is relatively close to the metal oxide surface, both in terms of spatial distance and the number of bonds in the linker group. This would favor rapid charge recombination. In **P_2-PZ**, the **PZ** linkage increases the through-space distance to the metal oxide, and reduces the through-bond coupling of the porphyrin radical cation to the metal oxide. Thus, charge recombination is expected to be slower for **P_2-PZ**, and this likely increases the cell efficiency.

In addition to the factors mentioned above, it is possible that **P_2-PZ** hinders the approach of the oxidized mediator (I_3^-) to the metal oxide surface, relative to the smaller **P**, and thus reduces the amount of charge recombination[32] due to reduction of I_3^- by electrons in the TiO_2. Aggregation of porphyrins or other sensitizers on the metal oxide surface has been shown to limit cell performance.[33-35] It is possible that such aggregation is reduced with **P_2-PZ** due to the angles at which the porphyrins are held and the presence of the dodecyloxy chains, and that this contributes as well to the performance increase.

Experimental

General

Tetrabutylammonium hexafluorophosphate was recrystallized twice from ethanol and dried under reduced pressure prior to use as the supporting electrolyte for electrochemical experiments. Fluorine doped tin oxide coated glass electrodes (TEC 15) were purchased from Hartford Glass Co. Hot melt sealing film used in constructing the DSSCs was purchased from Solaronix. *Meso*-(4-dodecyloxyphen-1-yl)-2,2'-dipyrromethane was prepared according to a reported literature

procedure.[36] Matrix assisted laser desorption/ionization time of flight (MALDI-TOF) mass spectra were determined using an Applied Biosystems Voyager-DE STR workstation and acquired in reflector mode using terthiophene, diphenylbutadiene or dithranol as the matrix. The NMR spectra were acquired using a Varian (Agilent) MR 400 MHz NMR spectrometer operating at an ^{1}H Larmor frequency of 399.87 MHz and equipped with a 5 mm broadband Z-gradient probe. The UV-visible spectra were acquired using a Shimadzu UV-2550 UV-visible spectrophotometer. Cyclic voltammograms were acquired using a CH Instruments 650C potentiostat. Photonic measurements used a 350 W Xe lamp from Osram, a Keithley 2400 source meter, and a Jobin-Yvon monochrometer.

Synthesis

Porphyrin 1. The synthesis of **1** was achieved via several steps, the products of which were not separated or characterized until reasonable differences in mobility using silica gel chromatography were observed. Portions of *p*-dodecyloxybenzaldehyde (5.0 g, 17.2 mmol), *meso*-(*p*-dodecyloxyphenyl)dipyrromethane (2.05 g, 5.05 mmol) and dipyrromethane (1.78 g, 12.2 mmol) were added to a 3 L round-bottomed flask containing deoxygenated $CHCl_3$ (2 L). EtOH (15 mL) and $BF_3{\cdot}OEt_2$ (0.454 mL, 3.62 mmol) were added and the reaction was left to stir in the dark for 3 h prior to addition of 2,3-dichloro-5,6-dicycanobenzoquinone (5.86 g, 25.8 mmol), following which stirring was continued for 1 h more. The solution was then passed through a thick pad of silica gel and concentrated, and the porphyrin product mixture was purified by silica gel chromatography (neat hexanes to hexanes/CH_2Cl_2 (1/1). The eluent was concentrated and then taken up in 500 mL of dichloromethane to which $Zn(AcO)_2{\cdot}2H_2O$ (9.45 g, 43.0 mmol) in MeOH (200 mL) was added. The solution was warmed to reflux overnight, cooled, and washed with water, and the organics were concentrated by removal of the solvent at reduced pressure and passed through a large pad of silica using dichloromethane/hexane (1/1) as the eluting solvent. Removal of the solvent by distillation at reduced pressure afforded a purple residue that was dissolved in $CHCl_3$ (0.5 L). *N*-Bromosuccinimide (NBS, 0.613 g, 3.44 mmol) was added and the mixture was stirred at ambient temperature in the dark for 2 h. The solution was concentrated by distillation at reduced pressure, and the residue was taken up in a minimal amount of dichloromethane and passed through a large silica gel pad with elution by dichloromethane. The brominated porphyrin mixture obtained was concentrated and dried under high vacuum in a 1 L round-bottomed flask. Portions of 1,2-dichloroethane (450 mL) and Et_3N (7.26 mL, 52 mmol) were added and argon was bubbled through the solution for 20 min after which $Pd(PPh_3)_2Cl_2$ (0.14 g, 0.20 mmol) and 4,4,5,5-tetramethyl-1,3,2-dioxaborolane (5.80 mL, 40 mmol) were added. The solution was warmed to reflux and stirred overnight under argon. The solution was then cooled and concentrated by removal of the solvent by distillation at reduced pressure and the residue was purified by silica gel chromatography using a gradient solvent system of dichloromethane/hexane (3/7 to 8/2), which allowed separation of the various products and isolation of 0.630g (0.492 mol, 9.7%) of porphyrin **1**. ^{1}H NMR (400 MHz, $CDCl_3$): δ 9.90 (d, J = 4.7 Hz, 2 H), 9.10 (d, J = 4.7 Hz, 2 H), 8.97 (m, 4 H), 8.08 (m, 6 H), 7.20 (m, 6 H), 4.15 (m, 6 H), 1.92 (m, 6 H), 1.84 (s, 12 H), 1.58 (m, 6 H), 1.50-1.21 (m, 48 H), 0.89 (m, 9 H). ^{13}C NMR (100 MHz, $CDCl_3$): δ 158.93, 158.89, 154.51, 150.92, 150.42, 149.78, 135.61, 135.49, 135.28, 135.17, 133.11, 132.78, 132.24, 131.59, 112.73, 112.70, 85.31, 68.47, 32.12, 29.89, 29.86, 29.85, 29.70, 29.56, 26.39, 25.50, 22.89, 14.31. MS (MALDI-TOF): m/z calcd 1277.766 $[M]^+$, obsd 1277.640.

Porphyrin-substituted phenanthrenedione 2. An oven-dried pressure tube containing a magnetic stirrer bar was charged with Cs_2CO_3 (0.192 g, 0.590 mmol), 3,6-dibromophenanthrenedione (7.2 mg, 0.197 mmol), **1** (0.630 g, 0.492 mmol) and freshly distilled THF (80 mL). Argon was bubbled through the solution for 20 min, following which, $Pd(PPh_3)_4$ (45.5 mg, 0.039 mmol) was added. The reaction tube was sealed with a Teflon screw cap and heated to 90 ^{o}C to stir overnight. On cooling, the solution was concentrated by distillation of the solvent under reduced pressure and the residue was purified by silica gel chromatography (dichloromethane/hexane, 4/1 to 9/1) and the solution was concentrated by distillation of the solvent under reduced pressure to yield **2** (0.338 g, 0.134mmol, 68%) as a shiny purple solid. ^{1}H NMR (400 MHz, $CDCl_3$ 55 ^{o}C): δ 8.84 (m, 18 H), 8.65 (d, J = 8 Hz, 2 H), 8.34 (d, J = 8 Hz, 2 H), 7.94 (m, 8 H), 7.73 (d, J = 8 Hz, 4 H), 7.14 (m, 8 H), 6.97 (d, J =8 Hz, 4 H), 4.15 (t, J = 6 Hz, 4 H), 4.10 (t, J = 6 Hz, 8 H), 1.89 (m, 12 H), 1.55 (m, 12 H), 1.50-1.22 (m, 96 H), 0.89 (m, 18 H). MS (MALDI-TOF): m/z calcd 2509.375 $[M]^+$, obsd 2509.553.

Dinitrile dye precursor 3. A 127 mg (50.6 μmol) portion of **3** and 24 mg (152 μmol) of 4,5-diaminophthalonitrile along with 20 mL of toluene, 10 mL of glacial acetic acid and 10 mL of ethanol were placed in a 100 mL round bottomed flask and heated at reflux for 20 h. The reaction solution was cooled, diluted with 100 mL of toluene and transferred to a separatory funnel. The solution was washed with 200 mL of water, and the organic layer collected, concentrated by distillation of the solvent at reduced pressure, and dried under high vacuum. The residue was taken up in dichloromethane, loaded onto a silica-gel column and chromatographed using dichloromethane/hexanes (3/2) as the eluting solvent. Appropriate fractions were concentrated, yielding 124 mg (46.8 μmol, 93%) of the desired product **3**. ^{1}H NMR (400 MHz, $CDCl_3$, 58 ^{o}C): δ 9.47 (d, J = 8.0 Hz, 2 H), 9.41 (s, 2 H), 8.83 (m, 16 H), 8.65 (d, J = 8.4 Hz, 2 H), 8.60 (d, J = 8.0 Hz, 2 H), 7.96 (m, 8 H), 7.69 (m, 4 H), 7.16 (m, 4 H), 7.09 (m, 4 H), 6.88 (m, 4 H), 4.16 (t, J = 6.8 Hz, 4 H), 4.00 (t, 6.4 Hz, 8 H), 1.91 (m, 4 H), 1.80 (m, 8 H), 1.56 (m, 4 H), 1.44 (m, 8 H), 1.28 (bs, 48 H), 0.864 (t, J = 7.2 Hz, 18 H).^{13}C NMR (100 MHz, $CDCl_3$): δ 159.21, 159.08, 151.00, 150.88, 150.59, 149.62, 147.81, 146.13, 141.39, 136.26, 135.62, 135.51, 135.07, 134.93, 132.72, 132.34, 132.17, 131.17, 131.27, 129.94, 128.67, 125.69, 121.83, 121.37, 119.08, 114.74, 112.97, 112.87, 112.69, 68.672, 68.55, 32.10, 29.87, 29.84, 29.82, 29.80, 29.78,

29.74, 29.69, 29.66, 29.51, 26.41, 26.35, 22.84, 14.18. MS (MALDI-TOF) m/z: calcd 2631.414 $[M]^+$, obsd 2630.157.

Sensitizer P_2-PZ. A 78.3 mg portion of **3** was dissolved in 50 mL of trifluoroacetic acid contained in an open pressure tube, 50 mL of 12.1 M HCl was added carefully and the tube was sealed quickly with a Teflon screw cap to limit loss of HCl gas evolved during the addition. The mixture was heated at reflux for 6 days after which it was cooled and transferred to a separatory funnel containing 300 mL of dichloromethane. The solution was neutralized with 3 M NaOH. The organic layer was isolated and washed further with saturated $NaHCO_3$ prior to concentration by distillation of the solvent at reduced pressure and drying at high vacuum overnight. MALDI-TOF analysis of the residue revealed that partial hydrolysis of the dodecyloxy groups had occurred. Consequently, the purple residue was taken up in 200 mL of dry dimethylformamide, and 0.25 g of K_2CO_3 was added, followed by 0.3 mL of 1-bromododecane. The solution was stirred at 70 ^oC overnight under argon, cooled, transferred into a separatory funnel containing 500mL H_2O and extracted with EtOAc. The organic layer was concentrated by distillation of the solvent, and the resulting purple residue was dissolved in 300 mL dichloromethane. A 65 mg portion of $ZnAcO_2{\cdot}H_2O$ dissolved in 50 mL of methanol was added and the solution was heated to reflux overnight. The dichloromethane solution was cooled, washed with water and concentrated prior to being dissolved in 200 mL of THF. A 1 g portion of KOH along with 20 mL of H_2O were added and the solution was heated at reflux for 16 h. The solution was cooled, carefully neutralized with 4 N hydrochloric acid and extracted with dichloromethane. Glacial acetic acid was added drop-wise to facilitate extraction. The isolated dichloromethane layer was washed with water, concentrated by distillation of the solvent under reduced pressure, and dried under high vacuum overnight. The residue was chromatographed on silica gel using dichloromethane followed by dichloromethane with 1 %, MeOH, then 4 % MeOH and finally 6% MeOH containing 1% AcOH to yield **P_2-PZ** (63 mg, 79%). ^{1}H NMR (400 MHz, 1,1,2,2-tetrachloroethane-d_6): δ 9.94 (d, J = 8 Hz, 2 H), 9.54 (m, 2 H), 9.16-8.63 (m, 18 H), 8.05 (m, 8 H), 7.79 (m, 4 H), 7.26 (m, 8 H), 7.00 (m, 4 H), 4.27 (m, 8 H), 4.08 (m, 4 H), 1.96 (m, 12 H), 1.66 (m, 12 H), 1.61-1.08 (m, 96 H), 0.96 (s, 18 H). MS (MALDI-TOF) m/z: calcd 2669.403 $[M]^+$, obsd 2669.518.

Free base methyl ester of porphyrin P. Chlororform (2.5 L) containing 18.75 mL of EtOH was deoxygenated with bubbling argon for 20 min. To this, 409 mg (2.49 mmol) of methyl 4-formyl benzoate, 2.025g (4.98 mmol) of *meso*-(4-dodecyloxyphen-1-yl)-2,2'-dipyrromethane and 0.724g (2.49 mmol) of 4-dodecyloxybenzaldehyde were added with stirring, followed by addition of 0.13 mL (1.047 mmol) $BF_3{\cdot}OEt_2$. The solution was allowed to stir in the dark under argon for 3 h following which 1.7 g (7.49 mmol) of 2,3-dichloro-5,6-dicycanobenzoquinone was added. Stirring was continued for 45 min. The solution was filtered through a thick pad of silica gel and concentrated by distillation of the solvent at reduced pressure, and the residue was purified using silica gel chromatography (hexane/dichloromethane, 1/1 to neat dichloromethane). Concentration of relevant fractions by distillation of the solvent under reduced pressure yielded 0.336 g (0.274 mmol, 11%) of the desired product. ^{1}H NMR (400 MHz, $CDCl_3$): δ 8.88 (d, J = 6 Hz, 6 H), 8.76 (d, J = 4 Hz, 2 H), 8.42 (d, J = 8 Hz, 2 H), 8.29 (d, J = 8 Hz, 2 H), 8.09 (d, J = 8 Hz, 2 H), 8.08 (d, J = 8 Hz, 4 H), 7.23 (d, J = 8 Hz, 6 H), 4.19 (t, J = 7 Hz, 6 H), 4.09 (s, 3 H), 1.95 (m, 6 H), 1.60 (m, 6 H), 1.31 (m, 54 H), 0.91 (t, J = 6 Hz, 9 H), -2.7 (s, 2 H). ^{13}C NMR (100 MHz, $CDCl_3$): δ 167.50, 159.17, 147.38, 135.84, 135.63, 134.89, 134. 45, 134.39, 129.62, 128.21, 127.87, 120.65, 120.31, 118.28, 113.11, 112.62, 68.71, 68.46, 68.21, 32.12, 29.89, 29.84, 29.65, 29.65, 29.56, 26.39, 22.88, 14.38, 14.23. MS (MALDI-TOF) m/z: calcd 1224.800 $[M]^+$, obsd 1224.914.

Free base of porphyrin P. A 90 mL portion of 2-propanol and 40 mL of 2 M aqueous KOH were added to a round bottomed flask containing 0.335 g (0.273 mmol) of the **free base methyl ester of porphyrin P**. The flask was fitted with a condenser and heated at reflux with stirring overnight. The solution was neutralized with 4 M aqueous HCl and extracted with dichloromethane. The organic layer was concentrated by distillation of the solvent at reduced pressure and dried under high vacuum to yield 0.291 g (0.24 mmol, 88%) of the desired carboxylic acid. ^{1}H NMR (400 MHz, $CDCl_3$): δ 8.89 (m, 6 H), 8.80 (d, J = 5 Hz, 2 H), 8.56 (d, J = 8 Hz, 2 H), 8.37 (d, J = 8 Hz, 2 H), 8.10 (m, 6 H), 7.26 (m, 6 H), 4.23 (m, 6 H), 1.97 (m, 6 H), 1.62 (m, 6 H), 1.54-1.16 (m, 48 H), 0.90 (t, J = 7 Hz, 9 H), -2.73 (s, 2 H). ^{13}C NMR (100 MHz, $CDCl_3$): δ 159.20, 159.19, 148.30, 135.74, 134.90, 134.47, 134.38, 128.70, 120.71, 120.36, 118.10, 112.90, 68.52, 32.11, 29.89, 29.85, 29.71, 29.68, 26.41, 22.88, 14.30. MS (MALDI-TOF) m/z: calcd 1210.785 $[M]^+$, obsd 1210.560.

Porphyrin P. A 0.187g portion of **5** (0.155 mmol) was taken up in 300 mL of dichloromethane to which 0.339 g (1.55 mmol) of $Zn(AcO)_2{\cdot}2H_2O$ dissolved in 30 mL of MeOH was added. The solution was heated at reflux overnight. The solution was diluted with 100 mL of dichloromethane and washed with water. The organic layer was concentrated by distillation of the solvent at reduced pressure and chromatographed on silica gel using 4% dichloromethane in MeOH as the solvent. A few drops of pyridine were added to prevent crystal formation at the silica gel solvent interface. Concentration of appropriate fractions by distillation of the solvent under reduced pressure and drying under high vacuum afforded 0.186 g of **P** (0.146 mmol, 94%). ^{1}H NMR (400 MHz, $CDCl_3$): δ 8.97 (d, J = 5 Hz, 2 H), 8.95 (bs, 4 H), 8.86 (d, J = 5 Hz, 2 H), 8.51 (d, J = 8 Hz, 2 H), 8.35 (d, J = 8 Hz, 2 H), 8.10 (d, J = 8 Hz, 6 H), 7.25 (m, 6 H), 4.23 (t, J = 7 Hz, 6 H), 1.97 (tt, J = 8 Hz, 6 H), 1.62 (tt, J = 8 Hz, 6 H), 1.53-1.20 (m, 48 H), 0.90 (t, J = 7 Hz, 9 H). ^{13}C NMR (100 MHz, $CDCl_3$): δ 171.5, 158.90, 150.84, 150.66, 150.59, 149.50, 150.44, 143.53, 135.61, 135.47, 135.44, 134.86, 132.35, 132.10, 131.98, 131.23, 128.42, 128.34, 122.36, 121.35, 121.03, 118.87, 112.64, 68.49, 32.12, 29.90, 29.85, 29.72, 29.56, 26.42, 22.88, 14.30. MS (MALDI-TOF) m/z: calcd 1272.698 $[M]^+$, obsd 1273.154.

Electrochemistry

A three-electrode setup contained in a one-compartment glass cell was used for cyclic voltammetry. A glassy carbon working electrode, platinum mesh counter electrode, and Ag^+/Ag quasi-reference were employed for all experiments. Experiments were performed in dichloromethane (distilled prior to use) solution containing 100 mM tetra-*n*-butylammonium hexafluorophosphate as the supporting electrolyte. The Ag^+/Ag quasi-reference electrode was prepared by polishing a silver wire and then exposing it to concentrated bleach solution for 1-2 min. After the formation of a Ag^+ coating as evidenced by a black tarnish, the wire was rinsed and used for the ensuing experiments. At the conclusion of experiments involving the analyte, ferrocene was introduced into the working solution and the potential of the ferrocenium/ferrocene (Fc^+/Fc) couple measured. Potentials are reported vs. SCE using a Fc^+/Fc potential of 0.45 V vs. SCE.

Dye-sensitized solar cells

The dye-sensitized solar cells were prepared followed methodologies established in the literature.[1,37] In brief, the transparent conducting fluorine doped tin oxide (FTO) based photoanodes were prepared by first applying a spray coating of an ethanolic solution of 0.2 M titanium acetylacetonate to form a ca. 100 nm thick TiO_2 layer[38] followed by treatment with $TiCl_4$,[37] deposition of a 6-8μm thick mesoporous TiO_2 layer,[39] and a final treatment with $TiCl_4$. The FTO-TiO_2 electrodes thus prepared were immersed in dichloromethane solutions of **P_2-PZ** or **P** overnight (>12 h) to yield finished photoanodes. The fully assembled solar cell consisted of this photoanode and an FTO-Pt cathode formed by applying a solution of chloroplatinic acid to an FTO surface and treating at 450 °C for 30 min. The two electrodes were sealed together using heat shrink plastic (Solaronix), and the electrolyte was introduced to the internal cavity of the cell via small ports drilled in the FTO-Pt cathode. The electrolyte consisted of 1:1 acetonitrile:valeronitrile with 0.2 M lithium iodide, 0.05 M iodine, 0.2 M tetrabutylammonium iodide, and 0.5 M 4-tertbutylpyridine.

Photocurrent and photovoltage measurements of the cells were obtained using a 350 W Xe lamp (Osram) with a 400 nm long pass filter (Thor Labs) and an AM 1.5 (Oriel) filter, with the cells positioned to receive a light intensity of 100 mW cm^{-2}. The geometric area of the cell exposed to illumination measured 0.20 cm^2. The incident photon to current efficiency (IPCE) measurements employed a Jobin-Yvon monochromator, with photocurrents measured in 4 nm intervals from 800 to 380 nm using a Keithley 2400 source meter. The intensity at each wavelength was determined with a Newport 818-UV photodiode in the same context as the DSSCs studied.

Conclusions

Above, we have presented a method for the synthesis of a new class of sensitizers for DSSC that employs two porphyrins and a pyrazine spacer. The spacer allows the two sensitizer dyes to be linked to the surface in the same molecule, and also provides two carboxylate groups to provide stronger binding to the metal oxide surface. The dodecyloxy groups enhance solubility and may hinder aggregation on the metal oxide surface. The new sensitizer provides slightly less maximum surface coverage than model porphyrin sensitizer **P**. This is likely because of the larger steric bulk of **P_2-PZ**. However, **P_2-PZ** gives considerably enhanced performance in the thin DSSC cells used here, which were designed to allow investigation of cell chemistry, rather than to maximize solar conversion efficiency. We speculate that this performance increase is mainly due to a reduced rate of charge recombination between the oxidized sensitizer and the TiO_2 surface, with a possible additional enhancement due to absorbance by the pyrazine linker moiety. More subtle surface effects might also play a role.

The structural motif illustrated by **P_2-PZ** allows embellishments, such as the use of two different porphyrins or other chromophores as sensitizers or antenna moieties in the same molecule. Such an approach would both fix the ratio of the two chromophores and assure the possibility of rapid and efficient energy or electron transfer between them. Increasing the length of the pyrazine linker could also bring new possibilities, such as actinic light absorption and/or active redox behavior as an electron relay.

Acknowledgments

This work was supported by the Office of Basic Energy Sciences, Division of Chemical Sciences, Geosciences, and Energy Biosciences, Department of Energy under contract DE-FG02-03ER15393 and the Center for Bio-Inspired Solar Fuel Production, an Energy Frontier Research Center funded by the U.S. Department of Energy, Office of Science, Office of Basic Energy Sciences under Award Number DE-SC0001016.

Notes and references

[a]*Department of Chemistry and Biochemistry, Arizona State University, Tempe, Arizona, 85287*

1 B. O'Regan and M. Graetzel, *Nature*, 1991**, 353**, 737-740.
2 A. Hagfeldt, G. Boschloo, L. Sun, L. Kloo, and H. Pettersson, *Chem. Rev.*, 2010**, 110**, 6595-6663.
3 S. Ardo and G. J. Meyer, *Chem. Soc. Rev.*, 2009**, 38**, 115
4 M. Gratzel, *J. Photochem. Photobiol. C-Photochem. Rev.*, 2003**, 4**, 145-153.
5 D. Cahen, G. Hodes, M. Gratzel, J. F. Guillemoles, and I. Riess, *J. Phys. Chem. B*, 2000**, 104**, 2053-2059.
6 A. Yella, H. W. Lee, H. N. Tsao, C. Yi, A. K. Chandiran, M. K. Nazeeruddin, E. W. G. Diau, C. Y. Yeh, S. M. Zakeeruddin, and M. Gratzel, *Science*, 2011**, 334**, 629-634.
7 M. Graetzel, *Acc. Chem. Res.*, 2009**, 42**, 1788-1798.
8 N. Robertson, *Angew. Chem. ,Int. Ed.*, 2006**, 45**, 2338-2345.
9 T. Horiuchi, H. Miura, K. Sumioka, and S. Uchida, *J. Am. Chem. Soc.*, 2004**, 126**, 12218-12219.
10 A. Mishra, M. K. Fischer, and P. Baeuerle, *Angew. Chem. ,Int. Ed.*, 2009**, 48**, 2474-2499.

11 F. Gao, Y. Wang, D. Shi, J. Zhang, M. Wang, X. Jing, R. Humphry-Baker, P. Wang, S. M. Zakeeruddin, and M. Graetzel, *J. Am. Chem. Soc.*, 2008**, 130**, 10720-10728.
12 K. Hara, T. Sato, R. Katoh, A. Furube, Y. Ohga, A. Shinpo, S. Suga, K. Sayama, H. Sugihara, and H. Arakawa, *J. Phys. Chem. B*, 2003**, 107**, 597-606.
13 S. Kim, J. K. Lee, S. O. Kang, J. Ko, J. Yum, S. Fantacci, F. De Angelis, D. Di Censo, M. Nazeeruddin, and M. Graetzel, *J. Am. Chem. Soc.*, 2006**, 128**, 16701-16707.
14 W. M. Campbell, A. K. Burrell, D. L. Officer, and K. W. Jolley, *Coord. Chem. Rev.*, 2004**, 248**, 1363-1379.
15 T. Kitamura, M. Ikeda, K. Shigaki, T. Inoue, N. A. Anderson, X. Ai, T. Q. Lian, and S. Yanagida, *Chem. Mater.*, 2004**, 16**, 1806-1812.
16 D. P. Hagberg, J. H. Yum, H. Lee, F. De Angelis, T. Marinado, K. M. Karlsson, R. Humphry-Baker, L. Sun, A. Hagfeldt, M. Graetzel, and M. Nazeeruddin, *J. Am. Chem. Soc.*, 2008**, 130**, 6259-6266.
17 W. Zeng, Y. Cao, Y. Bai, Y. Wang, Y. Shi, M. Zhang, F. Wang, C. Pan, and P. Wang, *Chem. Mater.*, 2010**, 22**, 1915-1925.
18 W. M. Campbell, K. W. Jolley, P. Wagner, K. Wagner, P. J. Walsh, K. C. Gordon, L. Schmidt-Mende, M. K. Nazeeruddin, Q. Wang, M. Grätzel, and D. L. Officer, *J. Phys. Chem. C*, 2007**, 111**, 11760-11762.
19 H. Imahori, T. Umeyama, and S. Ito, *Acc. Chem. Res.*, 2009**, 42**, 1809-1818.
20 C. W. Lee, H. P. Lu, C. M. Lan, Y. L. Huang, Y. R. Liang, W. N. Yen, Y. C. Liu, Y. S. Lin, E. W.-G. Diau, and C. Y. Yeh, *Chem. Eur. J.*, 2009**, 15**, 1403-1412.
21 T. Owen, in *Fundamentals of UV-visible spectroscopy*, Agilent Technologies, Germany, 2000, pp. 71.
22 E. Galoppini, *Coord. Chem. Rev.*, 2004**, 248**, 1283-1297.
23 L. Zhang and J. M. Cole, *ACS Appl. Mater. Interfaces*, 2015**, 7**, 3427-3455.
24 K. Ladomenou, T. Kitsopoulos, G. Sharma, and A. Coutsolelos, *Rsc Advances*, 2014**, 4**, 21379-21404.
25 F. Ambrosio, N. Martsinovich, and A. Troisi, *J. Phys. Chem. Lett.*, 2012**, 3**, 1531-1535.
26 B. G. Kim, K. Chung, and J. Kim, *Chem. Eur. J.*, 2013**, 19**, 5220-5230.
27 Y. Tachibana, S. A. Haque, I. P. Mercer, J. R. Durrant, and D. R. Klug, *J. Phys. Chem. B*, 2000**, 104**, 1198-1205.
28 Y. Tachibana, J. E. Moser, M. Gratzel, D. R. Klug, and J. R. Durrant, *J. Phys. Chem.*, 1996**, 100**, 20056-20062.
29 A. Hagfeldt and M. Graetzel, *Acc. Chem. Res.*, 2000**, 33**, 269-277.
30 D. Kuciauskas, S. Lin, G. R. Seely, A. L. Moore, T. A. Moore, D. Gust, T. Drovetskaya, C. A. Reed, and P. D. W. Boyd, *J. Phys. Chem.*, 1996**, 100**, 15926-15932.
31 M. J. Griffith, K. Sunahara, P. Wagner, K. Wagner, G. G. Wallace, D. L. Officer, A. Furube, R. Katoh, S. Mori, and A. J. Mozer, *Chem. Commun.*, 2012**, 48**, 4145-4162.
32 R. N. Sampaio, R. M. O'Donnell, T. J. Barr, and G. J. Meyer, *J. Phys. Chem. Lett.*, 2014**, 5**, 3265-3268.
33 H. P. Lu, C. Y. Tsai, W. N. Yen, C. P. Hsieh, C. W. Lee, C. Y. Yeh, and E. W.-G. Diau, *J. Phys. Chem. C*, 2009**, 113**, 20990-20997.
34 J. H. Yum, S. r. Jang, R. Humphry-Baker, M. Graetzel, J. J. Cid, T. Torres, and M. Nazeeruddin, *Langmuir*, 2008**, 24**, 5636-5640.
35 C. L. Wang, C. M. Lan, S. H. Hong, Y. F. Wang, T. Y. Pan, C. W. Chang, H. H. Kuo, M. Y. Kuo, E. W.-G. Diau, and C. Y. Lin, *Energy Environ. Sci.*, 2012**, 5**, 6933-6940.
36 R. Takahashi and Y. Kobuke, *J. Org. Chem.*, 2005**, 70**, 2745-2753.
37 S. Ito, T. N. Murakami, P. Comte, P. Liska, C. Graetzel, M. K. Nazeeruddin, and M. Graetzel, *Thin Solid Films*, 2008**, 516**, 4613-4619.
38 L. Kavan and M. Gratzel, *Electrochim. Acta*, 1995**, 40**, 643-652.
39 M. G. Kang, N. G. Park, Y. J. Park, K. S. Ryu, and S. H. Chang, *Sol. Energy Mater. Sol. Cells*, 2003**, 75**, 475-479.